BULLETIN OF THE POLISH ACADEMY OF SCIENCES
TECHNICAL SCIENCES, Vol. 74(5), 2026, Article number: 1623
DOI: 10.24425/bpasts.2026.1623



# The influence of damping on the dynamic stability of complex mechanical systems, as exemplified by a truck crane

**Sebastian GARUS[1]*, Justyna GARUS[1], Wojciech SOCHACKI[1], Marcin NABIAŁEK[2], Bartłomiej JEŻ[1], and Kinga JEŻ[3]**

[1] Faculty of Mechanical Engineering, Department of Mechanics and Fundamentals of Machinery Design, Czestochowa University of Technology, ul. J.H. Dąbrowskiego 73, 42-201 Częstochowa, Poland

[2] Faculty of Production Engineering and Materials Technology, Department of Physics, Częstochowa University of Technology, Armii Krajowej 19, 42-201 Częstochowa, Poland

[3] Faculty of Civil Engineering, Czestochowa University of Technology, ul. Akademicka 3, 42-201 Częstochowa, Poland

**Abstract.** This work aimed to model and analyze the dynamic stability of a truck crane boom change system, taking into account the effect of various types of vibration damping on its dynamic stability. The paper formulates and solves boundary-value problems for a truck crane boom change system, accounting for damping, using a real DST0285 truck crane boom change system modeled as Bernoulli-Euler beams and selected discrete elements. Using Hamilton's variational principle, the equation of motion of the system was obtained, and, taking into account geometric and continuity conditions, the natural boundary conditions were determined. The equation of motion was then transformed into the Mathieu equation, whose parameters allowed the determination of the system's stable solution range.

**Keywords:** mechanical vibrations; damping; dynamic stability; Mathieu equation.

## 1. INTRODUCTION

The luffing system of a truck crane is one of the key subsystems determining the crane dynamic properties. It plays a decisive role in the accuracy of load positioning and affects the operational stability of the entire crane.

Issues related to the dynamics of mobile cranes, including the modelling of telescopic booms and their drive systems, have been comprehensively discussed in monographs by Posiadała [1] and Sochacki [2]. Many other studies have analysed crane vibrations and the dynamic stability of the crane luffing system. For modelling the crane or selected subsystems, both beam models and discrete models have been employed. In paper [3], Cekus *et al.* developed a mathematical model of a crane to analyse the motion of a load carried by the crane, taking into account the influence of wind force. In the article [4], Trąbka presented ten variants of a computational model of a telescopic crane dynamics using the finite element method. The variants differed in the number and selection of flexible elements. The study analysed how these differences affect the representation of the real crane dynamic properties in its computational models. Sagirli *et al.* [5] presented a model of a telescopic crane using the bond graph technique. The model included both the drive system and the main structure, treating them as a single highly nonlinear system. Zheng and Wang in paper [6] conducted a kinematic and dynamic analysis of the motions of a telescopic-boom crane. The influence of slewing, luffing, and telescoping of the boom, as well as load hoisting and lowering, on the crane dynamics was examined. Esqué *et al.* [7] proposed a modular method for the design and testing of hydraulic mobile cranes. A 3D graphical interface was developed to visualise, in real time, simulation results of crane operation for virtual prototyping applications. Kjelland and Hansen in publication [8] proposed a method for active vibration control of a truck-mounted crane boom. Based on information about natural vibration frequencies and damping of a simplified crane model, an input-shaping scheme was developed to control the feedback of a proportional valve pressure, resulting in significant vibration reduction. Sochacki [9] proposed a model of a truck crane and its boom that enables the analysis of vibration frequencies and the determination of conditions leading to dynamic instability. Mijailović and Šelmić investigated the influence of modelling structural components, particularly bearing compliance, on the dynamic behaviour and stability of a truck crane [10, 11]. In paper [12], Sun and Kleeberger developed and applied an integrated method for the dynamic analysis of a mobile crane, in which a flexible multibody structural model was directly coupled with the model of the crane hydraulic drive and control system. Ilir and Naser, in turn, analysed key kinematic and dynamic parameters (velocities, accelerations, forces, and moments) in the main crane subsystems. The obtained results were used to assess the dynamic behaviour and to select and optimise motion-control strategies to reduce vibrations and improve the crane operating efficiency [13].

*e-mail: sebastian.garus@pcz.pl

Manuscript submitted 2026-02-28, revised 2026-05-18, initially accepted for publication 2026-06-08, published in September 2026.

There are also several studies focusing on incorporating various damping mechanisms into models of telescopic booms and entire cranes. Liu *et al.* in paper [14] investigated the dynamic stability of a telescopic crane boom. The boundary value problem was formulated based on Hamilton's principle. Regions of dynamic instability were determined, and the influence of damping on these regions was analysed. Bold *et al.* [15] analysed the effect of structural and material damping on the vibrations of a truck crane with a telescopic boom, indicating the critical role of damping in shaping the dynamic response and the boundaries of dynamic stability. Similar issues, with respect to telescopic booms, were addressed by Raftoyiannis and Mihaltsos in paper [16]. In the article [17], Mączyński and Wojciech presented a 3D model of a truck-mounted telescopic crane that included structural flexibility and damping effects. An optimisation of the slewing frame drive functions was performed to minimise load oscillations at the final positioning stage.

The extensive literature on cranes also includes works devoted to stability assessment in the context of safety criteria. Kacalak *et al.* [18] proposed a methodology for assessing the stability of cranes with telescopic booms by combining static and dynamic analyses to quantify the range of stability loss.

In turn, the study by Tran and Nguyen [19] concerns the identification of the dynamic stability of truck cranes using models that reflect real operating conditions. Mackojć and Chiliński [20] proposed a preliminary methodology for the dynamic modelling of a coupled payload–vessel system with an offshore crane, intended for the analysis of lifting operations involving loads of varying mass. The developed model accounts for dynamic interactions and enables the study of vibrations and system stability under real operating conditions. In the article [21], Qian *et al.* presented an interactive analysis method for the quantitative determination of support reaction forces in a hydraulic mobile crane. The study aimed to limit the crane load capacity to a range that ensures static stability.

Relatively few studies simultaneously consider a luffing-system model that includes internal, external, and structural damping, along with a comprehensive dynamic-stability analysis of this model.

In this paper, a comprehensive dynamic-stability analysis of the luffing system of a truck crane is conducted, accounting for three types of damping. The influence of internal damping of the viscoelastic material (Kelvin–Voigt type) of the system components on the vibrations and dynamic stability of the DST0285 truck crane luffing system is analysed. An analysis of the influence of external-medium damping on the system dynamic stability is also performed. Moreover, the study examines how the dynamic stability of the system is affected by structural damping in the mountings of the luffing cylinder and the telescopic boom to the rotating superstructure frame.

Modeling mechanical devices requires certain simplifications. Bernoulli-Euler beams are widely used to model complex, slender mechanical systems and their vibrations, and their properties are therefore continuously studied in many centers [22–25]. In addition, these beams are also used for modeling in the construction industry [26].

The results of the research on the dynamics of the DST 0285 crane boom change system for analytical and numerical models (FEM) and a laboratory model are presented, among others, in [27, 28].

The crane luffing system is modelled as a continuous–discrete system using Bernoulli–Euler beams and equivalent masses and stiffnesses representing the telescopic boom, the luffing cylinder, and the crane load. A complex mathematical model of the luffing system is formulated, for which the equations of motion and natural boundary conditions are derived using Hamilton's principle. The eigenvalues of the damped vibration system are determined. The influence of selected damping parameters and the load on the natural frequencies and the decay rates of vibration amplitudes is investigated. The effects of geometric parameters, loading, and damping on the system dynamic stability are then identified.

## 2. MATHEMATICAL MODEL

In this paper, the boundary-value problem for lateral vibrations of a truck-mounted crane boom change system in the boom-lift plane was formulated and solved. The physical model included energy dissipation in the supports attaching the crane to the chassis frame, the hydraulic cylinder, and the telescopic boom. Furthermore, the damping of the medium in which the crane is located and the internal damping of the viscoelastic material of the Bernoulli-Euler beams modeling the analyzed system (Kelvin-Voigt rheological model) were considered. The system under consideration was the boom change system of the DST0285 truck-mounted crane, the physical diagram of which is shown in Fig. 1.

The system shown in the diagram consists of a telescopic boom and a hydraulic cylinder modeled using Bernoulli-Euler beams (Fig. 2). The hydraulic cylinder consists of a cylinder (b) whose modeling beams are described by the indices *1* and *2*, and a piston rod (a) modeled by beams designated *3* and *4*, respectively, where $l_2 = l_3$. The coefficient $k_1$ models the stiffness of the fluid in the cylinder (c) as a linear translational spring. The axial force $P_2(t)$ is equal to zero because the external load is not transferred to this part of the actuator cylinder. This is the part of the cylinder not filled with hydraulic fluid at a given piston rod position. The beam elements designated *5* and *6* are a beam model of an actual three-link telescopic boom of a truck crane, the equivalent mass of which is modeled by a discrete element $M_Z$. Energy dissipation in the considered system occurs as a result of external viscous damping with a damping coefficient $C_E$, resistance to motion in the supports modeled by viscous rotational dampers with damping coefficients $C_{R1}$ and $C_{R2}$ for the boom support and the boom change actuator, respectively, and through internal damping characterized by the material viscosity coefficients $E_i^*$. Lifting or stopping a load of mass $m$ suspended on a rope during lowering loads the system with an external force in the form $P(t) = P_0 + S\cos\nu t$, where $P_0 = m\,g$ is the constant part of the load, while $S$ is the variable part of the load. The corresponding longitudinal forces for individual beams take the form

$$P_6(t) = P_5(t) - P_4(t)\cos\gamma = (P_0 + S\cos\nu t)\sin\varphi, \tag{1}$$

$$P_1(t) = P_3(t) = P_4(t) = (P_0 + S\cos\nu t)\left(1 + \frac{l_6}{l_5}\right)\frac{\cos\varphi}{\sin\gamma}. \tag{2}$$

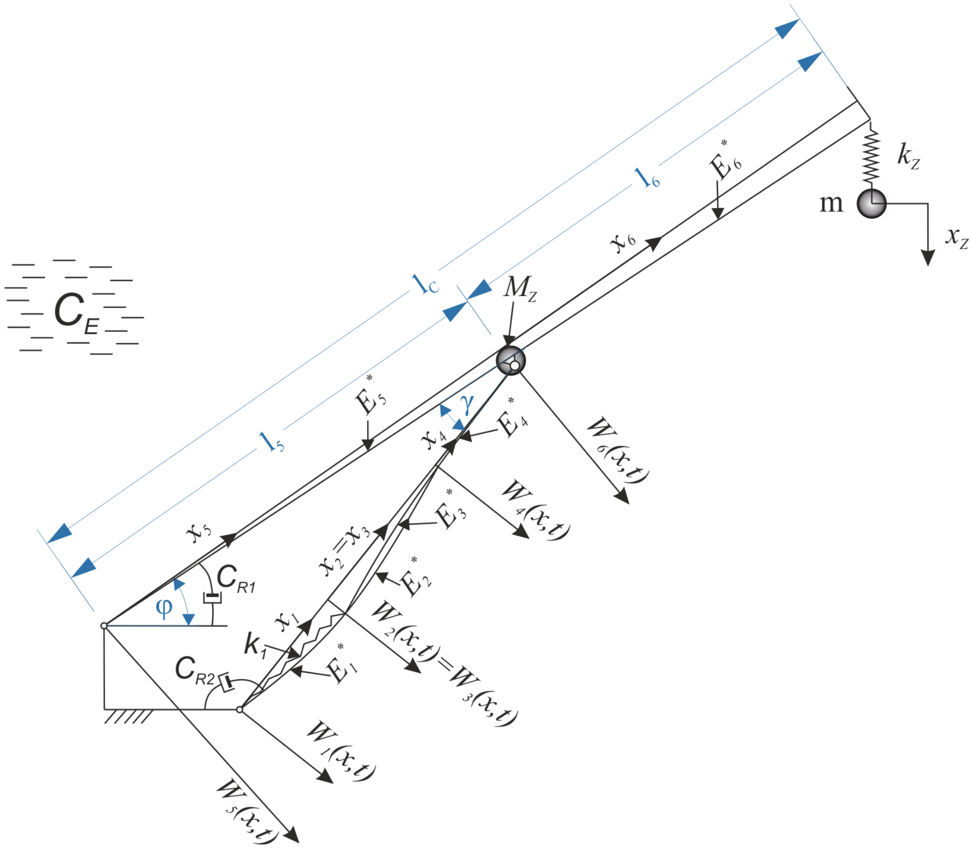


**Fig. 1.** Model of the boom change system of the DST0285 truck crane

The elasticity of a linear system is modeled by the spring coefficient $k_Z$. The angles $\varphi$ and $\gamma$ define the geometry of the system. The problem of lateral vibrations of the system was solved using Hamilton's variational principle for non-conservative systems, which can be represented as

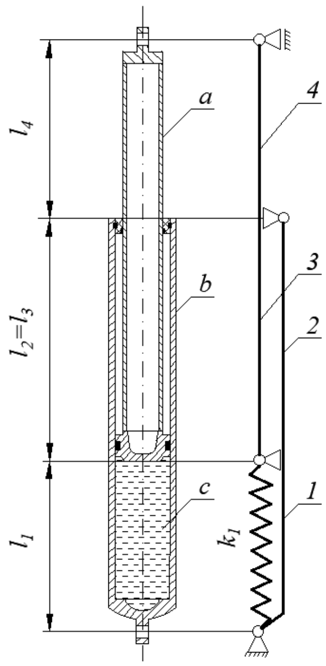


**Fig. 2.** Diagram and model of the boom change actuator

$$\int_{t_1}^{t_2} (\delta T - \delta V)\,\mathrm{d}t + \int_{t_1}^{t_2} \delta W_N\,\mathrm{d}t = 0. \tag{3}$$

The integral of the action is presented by

$$\begin{aligned}\int_{t_1}^{t_2} (T - V)\,\mathrm{d}t = \int_{t_1}^{t_2} \Bigg[ & \frac{1}{2}\sum_{i=1}^{6}\int_0^{l_i} \varrho_i A_i \left(\frac{\partial W_i(x_i,t)}{\partial t}\right)^2 \mathrm{d}x_i \\ & + \frac{1}{2} M_Z \left(\frac{\partial W_6(0,t)}{\partial t}\right)^2 + \frac{1}{2} m \left(\frac{\partial x_Z(t)}{\partial t}\right)^2 \\ & - \frac{1}{2}\sum_{i=1}^{6}\int_0^{l_i} E_i J_i \left(\frac{\partial^2 W_i(x_i,t)}{\partial x_i^2}\right)^2 \mathrm{d}x_i \\ & - \frac{1}{2}\sum_{i=1,3,4,5,6}\int_0^{l_i} P_i(t) \left(\frac{\partial W_i(x_i,t)}{\partial x_i}\right)^2 \mathrm{d}x_i \\ & - \frac{1}{2} k_1 \left[W_6(0,t)\sin\gamma\right]^2 \\ & - \frac{1}{2} k_Z \left[x_Z(t) - W_6(l_6,t)\cos\varphi\right]^2 \Bigg] \mathrm{d}t. \end{aligned} \tag{4}$$

The variation of the kinetic energy of the system $\delta T$ was, after applying appropriate transformations and using the relationship that $\delta w_i(x_i,t) = 0$ at $t = t_1$ and $t = t_2$, where $n$ is the number of beam elements in the system, defined by

$$\begin{aligned}\delta T = &-\sum_{i=1}^{n} \varrho_i A_i \int_{t_1}^{t_2} \frac{\partial}{\partial t}\left(\frac{\partial W_i(x_i,t)}{\partial t}\right)\delta W_i(x_i,t)\,\mathrm{d}t \\ &- M_Z \int_{t_1}^{t_2} \frac{\partial^2 W_6(0,t)}{\partial t^2}\delta W_6(0,t)\,\mathrm{d}t \\ &- m\int_{t_1}^{t_2} \frac{\partial^2 x_Z(t)}{\partial t^2}\delta x_Z(t)\,\mathrm{d}t. \end{aligned} \tag{5}$$

The variation of the potential energy of the system $\delta V$ was defined as

$$\begin{aligned}\delta V = \sum_{i=1}^{n} \Bigg[ &E_i J_i \frac{\partial^2 W_i(x_i,t)}{\partial x_i^2}\,\delta \frac{\partial W_i(x_i,t)}{\partial x_i}\Bigg|_{x_i=0}^{x_i=l_i} \\ &- E_i J_i \frac{\partial^3 W_i(x_i,t)}{\partial x_i^3}\delta W_i(x_i,t)\Bigg|_{x_i=0}^{x_i=l_i} \\ &+ E_i J_i \int_0^{l_i} \frac{\partial^4 W_i(x_i,t)}{\partial x_i^4}\delta W_i(x_i,t)\,\mathrm{d}x_i \\ &- P_i(t)\frac{\partial W_i(x_i,t)}{\partial x_i}\delta W_i(x_i,t)\Bigg|_{x_i=0}^{x_i=l_i} \\ &+ P_i(t)\int_0^{l_i} \frac{\partial^2 W_i(x_i,t)}{\partial x_i^2}\delta W_i(x_i,t)\,\mathrm{d}x_i \Bigg] \\ &+ k_1 \sin\gamma W_6(0,t)\delta\left(W_6(0,t)\sin\gamma\right) + k_Z\left(x_Z(t)\right. \\ &\left.- W_6\left(l_6,t\right)\cos\varphi\right)\left(\delta x_Z(t) - \delta W_6\left(l_6,t\right)\cos\varphi\right). \end{aligned} \tag{6}$$

The variation of the virtual work of non-conservative forces $\delta W_N$ was determined as

$$\begin{aligned}\delta W_N = \sum_{i=1}^{n} \Bigg\{ &-\int_0^{l_i} E_i{}^* J_i \frac{\partial^5 W_i(x_i,t)}{\partial x_i^4 \partial t}\delta W_i(x_i,t)\,\mathrm{d}x_i \\ &-\int_0^{l_i} C_E \frac{\partial W_i(x_i,t)}{\partial t}\delta W_i(x_i,t)\,\mathrm{d}x_i \Bigg\} \\ &- C_{R1}\frac{\partial^2 W_5(0,t)}{\partial x_5 \partial t}\delta \frac{\partial W_5(0,t)}{\partial x_5} \\ &- C_{R2}\frac{\partial^2 W_1(0,t)}{\partial x_1 \partial t}\delta \frac{\partial W_1(0,t)}{\partial x_1} \\ &-\sum_{i=1}^{n}\Bigg\{ E_i{}^* J_i \frac{\partial^3 W_i(x_i,t)}{\partial x_i^2 \partial t}\delta \frac{\partial W_i(x_i,t)}{\partial x_i}\Bigg|_{x_i=0}^{x_i=l_i} \\ &- E_i{}^* J_i \frac{\partial^4 W_i(x_i,t)}{\partial x_i^3 \partial t}\delta W_i(x_i,t)\Bigg|_{x_i=0}^{x_i=l_i}\Bigg\}. \end{aligned} \tag{7}$$

The individual variational components resulting from Hamilton's principle was determined by substituting equations (5), (6) and (7) into (3), from which the boundary conditions were then obtained, are as follows

$$\begin{aligned} &\int_{t_1}^{t_2}\Bigg(\int_0^{l_i}\Bigg(\sum_{i=1}^{n}\Bigg\{-E_i{}^* J_i \frac{\partial^5 W_i(x_i,t)}{\partial x_i^4 \partial t} - E_i J_i \frac{\partial^4 W_i(x_i,t)}{\partial x_i^4} \\ &-P_i(t)\frac{\partial^2 W_i(x_i,t)}{\partial x_i^2} - \varrho_i A_i \frac{\partial^2 W_i(x_i,t)}{\partial t^2} - C_E \frac{\partial W_i(x_i,t)}{\partial t}\Bigg\}\Bigg) \\ &\cdot\ \delta W_i(x_i,t)\,\mathrm{d}x_i + \sum_{i=1}^{n}\left(-E_i J_i \frac{\partial^2 W_i(x_i,t)}{\partial x_i^2} - E_i{}^* J_i \frac{\partial^3 W_i(x_i,t)}{\partial x_i^2 \partial t}\right) \\ &\cdot\ \delta \frac{\partial W_i(x_i,t)}{\partial x_i}\Bigg|_{x_i=0}^{x_i=l_i} - \sum_{i=1}^{n}\Bigg\{E_i J_i \frac{\partial^3 W_i(x_i,t)}{\partial x_i^3} \\ &+ P_i(t)\frac{\partial W_i(x_i,t)}{\partial x_i} + E_i{}^* J_i \frac{\partial^4 W_i(x_i,t)}{\partial x_i^3 \partial t}\Bigg\}\delta W_i(x_i,t)\Bigg|_{x_i=0}^{x_i=l_i} \\ &-\left(k_1\left(\sin\gamma\right)^2 W_6(0,t) + M_Z \frac{\partial^2 W_6(0,t)}{\partial t^2}\right)\delta W_6(0,t) \\ &+\Big(k_Z\left(x_Z(t) - W_6(l_6,t)\cos\varphi\right)\Big)\cos\varphi\,\delta W_6(l_6,t) \\ &-\ C_{R1}\frac{\partial^2 W_5(0,t)}{\partial x_5 \partial t}\delta \frac{\partial W_5(0,t)}{\partial x_5} - C_{R2}\frac{\partial^2 W_1(0,t)}{\partial x_1 \partial t}\delta \frac{\partial W_1(0,t)}{\partial x_1} \\ &-\left(m\frac{\partial^2 x_Z(t)}{\partial t^2} + k_Z\big(x_Z(t) - W_6(l_6,t)\cos\varphi\big)\right)\delta x_Z(t)\Bigg)\,\mathrm{d}t = 0. \end{aligned} \tag{8}$$

The system of differential equations of motion of the transverse vibrations of the model was determined from (8) as

$$\begin{aligned}\frac{\partial^4 W_i(x_i,t)}{\partial x_i^4} + \frac{E_i{}^* J_i}{E_i J_i}\frac{\partial^5 W_i(x_i,t)}{\partial x_i^4 \partial t} + \frac{P_i(t)}{E_i J_i}\frac{\partial^2 W_i(x_i,t)}{\partial x_i^2} \\ + \frac{\varrho_i A_i}{E_i J_i}\frac{\partial^2 W_i(x_i,t)}{\partial t^2} + \frac{C_E}{E_i J_i}\frac{\partial W_i(x_i,t)}{\partial t} = 0. \end{aligned} \tag{9}$$

Based on Fig. 1, the geometric boundary conditions and continuity conditions of the system are as follows

$$W_1(0,t) = 0, \tag{10}$$

$$W_1(l_1,t) = W_2(0,t), \tag{11}$$

$$\frac{\partial W_1(l_1,t)}{\partial x_1} = \frac{\partial W_2(0,t)}{\partial x_2}, \tag{12}$$

$$W_2(0,t) = W_3(0,t), \tag{13}$$

$$W_2(l_2,t) = W_3(l_3,t), \tag{14}$$

$$W_3(l_3,t) = W_4(0,t), \tag{15}$$

$$\frac{\partial W_3(l_3,t)}{\partial x_3} = \frac{\partial W_4(0,t)}{\partial x_4}, \tag{16}$$

$$W_5(0,t) = 0, \tag{17}$$

$$W_5(l_5,t) = W_6(0,t), \tag{18}$$

$$\frac{\partial W_5(l_5,t)}{\partial x_5} = \frac{\partial W_6(0,t)}{\partial x_6}, \tag{19}$$

$$W_4(l_4,t) = W_6(0,t)\cos\gamma. \tag{20}$$

Taking into account the geometric and continuity conditions, the natural boundary conditions were determined from (8) in the form

$$E_1J_1\frac{\partial^2 W_1(0,t)}{\partial x_1^2}+E_1{}^*J_1\frac{\partial^3 W_1(0,t)}{\partial x_1^2\partial t}=-C_{R2}\frac{\partial^2 W_1(0,t)}{\partial x_1\partial t}, \quad (21)$$

$$E_2J_2\frac{\partial^2 W_2(l_2,t)}{\partial x_2^2}+E_2{}^*J_2\frac{\partial^3 W_2(l_2,t)}{\partial x_2^2\partial t}=0, \quad (22)$$

$$E_1J_1\frac{\partial^2 W_1(l_1,t)}{\partial x_1^2}+E_1{}^*J_1\frac{\partial^3 W_1(l_1,t)}{\partial x_1^2\partial t} = E_2J_2\frac{\partial^2 W_2(0,t)}{\partial x_2^2}+E_2{}^*J_2\frac{\partial^3 W_2(0,t)}{\partial x_2^2\partial t}, \quad (23)$$

$$E_3J_3\frac{\partial^2 W_3(0,t)}{\partial x_3^2}+E_3{}^*J_3\frac{\partial^3 W_3(0,t)}{\partial x_3^2\partial t}=0, \quad (24)$$

$$E_3J_3\frac{\partial^2 W_3(l_3,t)}{\partial x_3^2}+E_3{}^*J_3\frac{\partial^3 W_3(l_3,t)}{\partial x_3^2\partial t} = E_4J_4\frac{\partial^2 W_4(0,t)}{\partial x_4^2}+E_4{}^*J_4\frac{\partial^3 W_4(0,t)}{\partial x_4^2\partial t}, \quad (25)$$

$$E_4J_4\frac{\partial^2 W_4(l_4,t)}{\partial x_4^2}+E_4{}^*J_4\frac{\partial^3 W_4(l_4,t)}{\partial x_4^2\partial t}=0, \quad (26)$$

$$E_5J_5\frac{\partial^2 W_5(0,t)}{\partial x_5^2}+E_5{}^*J_5\frac{\partial^3 W_5(0,t)}{\partial x_5^2\partial t} = -C_{R1}\frac{\partial^2 W_5(0,t)}{\partial x_5\partial t}, \quad (27)$$

$$E_5J_5\frac{\partial^2 W_5(l_5,t)}{\partial x_5^2}+E_5{}^*J_5\frac{\partial^3 W_5(l_5,t)}{\partial x_5^2\partial t} = E_6J_6\frac{\partial^2 W_6(0,t)}{\partial x_6^2}+E_6{}^*J_6\frac{\partial^3 W_6(0,t)}{\partial x_6^2\partial t}, \quad (28)$$

$$E_6J_6\frac{\partial^2 W_6(l_6,t)}{\partial x_6^2}+E_6{}^*J_6\frac{\partial^3 W_6(l_6,t)}{\partial x_6^2\partial t}=0, \quad (29)$$

$$\begin{aligned}E_1J_1&\frac{\partial^3 W_1(l_1,t)}{\partial x_1^3}+P_1(t)\frac{\partial W_1(l_1,t)}{\partial x_1}\\&+E_1{}^*J_1\frac{\partial^4 W_1(l_1,t)}{\partial x_1^3\partial t}-E_2J_2\frac{\partial^3 W_2(0,t)}{\partial x_2^3}\\&-E_2{}^*J_2\frac{\partial^4 W_2(0,t)}{\partial x_2^3\partial t}-E_3J_3\frac{\partial^3 W_3(0,t)}{\partial x_3^3}\\&-E_3{}^*J_3\frac{\partial^4 W_3(0,t)}{\partial x_3^3\partial t}-P_3(t)\frac{\partial W_3(0,t)}{\partial x_3}=0,\end{aligned} \quad (30)$$

$$\begin{aligned}E_2J_2&\frac{\partial^3 W_2(l_2,t)}{\partial x_2^3}+E_2{}^*J_2\frac{\partial^4 W_2(l_2,t)}{\partial x_2^3\partial t}\\&+E_3J_3\frac{\partial^3 W_3(l_3,t)}{\partial x_3^3}+E_3{}^*J_3\frac{\partial^4 W_3(l_3,t)}{\partial x_3^3\partial t}\\&-E_4J_4\frac{\partial^3 W_4(0,t)}{\partial x_4^3}-E_4{}^*J_4\frac{\partial^4 W_4(0,t)}{\partial x_4^3\partial t}=0,\end{aligned} \quad (31)$$

$$\begin{aligned}E_6J_6&\frac{\partial^3 W_6(l_6,t)}{\partial x_6^3}+E_6{}^*J_6\frac{\partial^4 W_6(l_6,t)}{\partial x_6^3\partial t}+P_6(t)\frac{\partial W_6(l_6,t)}{\partial x_6}\\&=-\left(k_Z\left(x_Z(t)-W_6(l_6,t)\cos\varphi\right)\right)\cos\varphi,\end{aligned} \quad (32)$$

$$\begin{aligned}E_5J_5&\frac{\partial^3 W_5(l_5,t)}{\partial x_5^3}+E_5{}^*J_5\frac{\partial^4 W_5(l_5,t)}{\partial x_5^3\partial t}\\&-E_6J_6\frac{\partial^3 W_6(0,t)}{\partial x_6^3}-E_6{}^*J_6\frac{\partial^4 W_6(0,t)}{\partial x_6^3\partial t}\\&+\left[E_4J_4\frac{\partial^3 W_4(l_4,t)}{\partial x_4^3}+E_4{}^*J_4\frac{\partial^4 W_4(l_4,t)}{\partial x_4^3\partial t}\right.\\&\left.+P_4(t)\frac{\partial W_4(l_4,t)}{\partial x_4}\right]\cos\gamma\\&-k_1\left(\sin\gamma\right)^2 W_6(0,t)-M_Z\frac{\partial^2 W_6(0,t)}{\partial t^2}=0,\end{aligned} \quad (33)$$

$$m\frac{\partial^2 x_Z(t)}{\partial t^2}+k_Z\left(x_Z(t)-W_6(l_6,t)\cos\varphi\right)=0. \quad (34)$$

To determine the eigenfunctions, the problem of system vibrations should be solved assuming that the variable part of the load $S$ is equal to 0. To separate variables in equation (9) and in the boundary conditions, equations (10)–(34), $W_i(x_i,t)=w_i(x_i)e^{j\omega t}$ and $x_Z(t)=x_Ze^{j\omega t}$ were assumed. The equation of motion after separation of variables takes the form

$$\frac{\partial^4 w_i(x_i)}{\partial x_i^4}+d_i^2\frac{\partial^2 w_i(x_i)}{\partial x_i^2}-\Omega_i^2 w_i(x_i)=0, \quad (35)$$

where $d_i=\sqrt{\dfrac{P_i}{E_iJ_i+j\omega E_i{}^*J_i}}$ and $\Omega_i=\sqrt{\dfrac{\varrho_iA_i\omega^2-j\omega C_E}{E_iJ_i+j\omega E_i{}^*J_i}}$.

The general solutions of the system of displacement equations (35) are the functions

$$\begin{aligned}w_i(x_i)&=C_{i1}\cosh\left(\alpha_ix_i\right)+C_{i2}\sinh\left(\alpha_ix_i\right)\\&+C_{i3}\cos\left(\beta_ix_i\right)+C_{i4}\sin(\beta_ix_i),\end{aligned} \quad (36)$$

where $C_{ik}$ for $k=\{1,2,3,4\}$ the integration constants and $\alpha_i$ and $\beta_i$ take the form

$$\alpha_i=\sqrt{-\frac{1}{2}d_i^2+\sqrt{\frac{1}{4}d_i^4+\Omega_i^2}}, \quad (37)$$

$$\beta_i=\sqrt{\frac{1}{2}d_i^2+\sqrt{\frac{1}{4}d_i^4+\Omega_i^2}}. \quad (38)$$

By inserting the solution (36) into equations (10)–(34) after separation of variables, a homogeneous system of equations $A$ with respect to unknown constants $C_{ik}$ was obtained. This system in matrix form was written as

$$\left[\mathbf{A}\right](\omega)\,\mathbf{C} = 0, \tag{39}$$

where $\left[\mathbf{A}\right](\omega) = \left[a_{p,q}\right]$; $[p,q] = (1–24)$, and $\mathbf{C} = [C_{ik}]^T$; $i = 1, 2, \ldots, 6$; $k = \{1,2,3,4\}$.

$$\det \mathbf{A}(\omega) = 0. \tag{40}$$

If, for constants $C_{ik}$, the determinant of the coefficient matrix is equal to zero (equation (40)), then the system has a non-trivial solution. Equation (40) allows the calculation of the eigenvalues of the system $\omega$. The calculated eigenvalues were in turn the basis for determining the eigenfunctions of the system under study.

To analyze the dynamic stability of the tested system, its equation of motion (equation (9)) should be presented in the form of the damped Mathieu equation, which takes the form

$$\frac{\partial^2 T(\tau)}{\partial \tau^2} + c\frac{\partial T(\tau)}{\partial \tau} + \left(\delta + \epsilon \cos t\right) T(\tau) = 0, \tag{41}$$

where $\tau$ is is dimensionless time, $T(\tau)$ is the time function of the vibration amplitude (generalized modal coordinate), and

$$c = \frac{C_E}{\nu^2 \sum\limits_{i=1}^{n} \varrho_i A_i} + \frac{\sum\limits_{i=1}^{n} E_i{}^* J_i \int\limits_0^{l_i} \frac{\partial^4 w_i(x_i)}{\partial x_i^4} w_i(x_i)\,\mathrm{d}x_i}{\nu^2 \sum\limits_{i=1}^{n} \varrho_i A_i \int\limits_0^{l_i} w_i^2(x_i)\,\mathrm{d}x_i}, \tag{42}$$

$$\delta = \frac{\omega^2}{\nu^2} - \frac{j\omega C_E}{\nu^2 \sum\limits_{i=1}^{n} \varrho_i A_i} - \frac{j\omega \sum\limits_{i=1}^{n} E_i{}^* J_i \int\limits_0^{l_i} \frac{\partial^4 w_i(x_i)}{\partial x_i^4} w_i(x_i)\,\mathrm{d}x_i}{\nu^2 \sum\limits_{i=1}^{n} \varrho_i A_i \int\limits_0^{l_i} w_i^2(x_i)\,\mathrm{d}x_i}, \tag{43}$$

$$\epsilon = \frac{S \sum\limits_{i=1}^{n} \int\limits_0^{l_i} \frac{\partial^2 w_i(x_i)}{\partial x_i^2} w_i(x_i)\,\mathrm{d}x_i}{\nu^2 \sum\limits_{i=1}^{n} \varrho_i A_i \int\limits_0^{l_i} w_i^2(x_i)\,\mathrm{d}x_i}. \tag{44}$$

Reducing the partial equations of a beam loaded by a periodic axial force to a Mathieu-type equation, via a modal expansion and the Galerkin procedure, is a classical procedure used in the dynamic stability analysis of elastic systems. This approach stems from Bolotin's theory and has been extensively applied to Bernoulli–Euler beams subjected to harmonic axial loading [29, 30].

Determining the numerical values of the parameters described by the relations (42), (43) and (44) allows us to determine the possibility of loss of dynamic stability of the tested system.

Figure 3 shows the effect of the $c$ coefficient on the range of stable solutions from the Mathieu equation (41). For the value of $c = 0.1$, the region of stable solutions is marked in gray. Increasing the $c$ coefficient to 0.3 increases the region for which the equation solutions are stable. Further increasing the $c$ parameter to values of 0.6 and 0.9 reduces the range of unstable solutions by the areas marked in yellow and blue in Fig. 3.

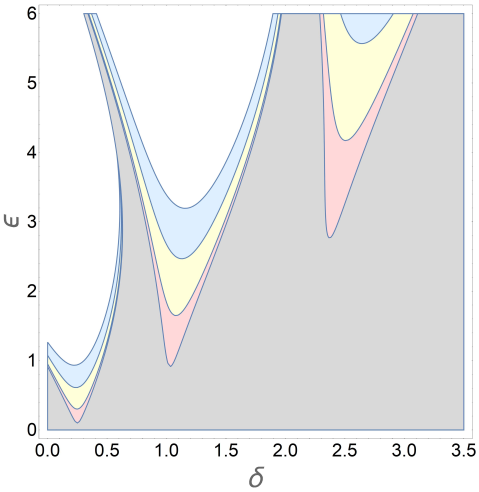


**Fig. 3.** The effect of damping on the increase of the areas of stable solutions of the Mathieu equation (Strutt card) for $c = 0.1$ (gray), $c = 0.3$ (red), $c = 0.6$ (yellow) and $c = 0.9$ (blue)

## 3. NUMERICAL RESULTS

This paper analyzes the boom change system of a DST0285 truck-mounted crane, the model of which is presented in Fig. 1. The boom change system consists of a boom change actuator, a mechanical cable system, and a three-link telescopic boom. The boom is composed of a fixed member and two extendable members.

The analyzed physical model of the system takes into account important features of the actual object, such as the stepwise stiffness variation of the beam modeling the telescopic boom, the geometry of the system defined by the geometric relationship between the angles $\varphi$ and $\gamma$, the effect of the force on the boom head resulting from the action of the load suspended on the cable, the effect of the hydraulic fluid of the boom change actuator on the vibrations of the system, modeling it through a flexible piston rod mount, and the effect of the boom mass on the vibrations of the analyzed system.

The following simplifications were adopted in the model:

- the ground on which the truck crane stands and its chassis are non-deformable,

- the body's rotating frame can only rotate around the chassis' vertical axis and is non-deformable,
- the boom rotation angle does not affect its dynamics,
- the piston rod of the boom change actuator is a beam system elastically supported in the longitudinal direction,
- shear deformation and rotary inertia effects were considered negligible.

A load that stops during descent or is lifted and vibrates vertically applies a pulsating force to the boom-changing system at a specific frequency. This frequency depends on the elasticity of the rope system and the mass of the load suspended from the rope. In this study, a six-strand rigging system was assumed, accounting for the stiffness of the strands from the head to the block and from the head to the winch.

The equivalent stiffness of the rope system was determined as

$$k_z = \frac{n^2 A_l E_l}{l_0 + n l_l}, \tag{45}$$

where
$n$ – number of rope strands (assumed $n = 6$),
$E_l$ – Young's modulus for the rope material ($E_l = 1.25 \cdot 10^{11}$ Pa),
$A_l$ – rope cross-section (where the strand diameter is $d = 0.016$ m),
$l_0$ – rope length from the boom head to the winches,
$l_l$ – length of rigging from the boom head to the block.

Considering the mass $m$ of the load and the equivalent stiffness of the cable system (45), the excitation frequency $\nu$ was determined as

$$\nu = \sqrt{\frac{k_z}{m}}. \tag{46}$$

Assuming the actual lowering (lifting) speeds of the load $v_0$, the excitation frequency $\nu$, and the equivalent stiffness of the cable system $k_z$, the variable part of the load $S$ can be determined as

$$S = k_z \sqrt{\frac{v_0^2}{\nu^2}}. \tag{47}$$

The determined value of the variable part of the load $S$ was used to determine the total parametric load of the tested system.

To investigate the effect of various types of damping on the eigenvalues of the crane boom change system, dimensionless damping coefficients were introduced. For internal damping $H_s$, external damping $N_s$, and structural damping $M_s$, respectively, as

$$H_s = \frac{{E_i}^*}{E_i \sqrt{\left(l_1 + \sum_{i=3}^{6} l_i\right)^4 \frac{\sum_{i=1}^{6} \varrho_i A_i}{\sum_{i=1}^{6} E_i J_i}}}, \tag{48}$$

$$N_s = \frac{C_E}{\sqrt{\sum_{i=1}^{6} \varrho_i A_i E_i J_i}} \left(l_1 + \sum_{i=3}^{6} l_i\right)^2, \tag{49}$$

$$M_s = \frac{C_R}{\sqrt{\left(l_1 + \sum_{i=3}^{6} l_i\right)^2 \sum_{i=1}^{6} \varrho_i A_i E_i J_i}}. \tag{50}$$

If the load on the crane is jerked or suddenly stopped while lowering, it will generate a time-varying external force $P(t)$, which consists of a constant $P_0$ and a variable $S$ component of the load. Both components depend on the boom inclination angle $\varphi$. The constant component is influenced by the mass $m$ of the suspended load, which, together with the equivalent stiffness of the cable system, defined by equation (45), also determines the frequency of the excitation force (equation (46)). The variable component of the load $S$ is related to the stiffness of the cable system $k_z$, the load lowering or lifting speed $v_0$, and the excitation frequency $\nu$ and is described by equation (47).

The equation of motion for the truck crane boom change system (9), presented in the form of the damped Mathieu equation (41), allows for determining the dynamic stability of the analyzed model. The pair of parameters $\delta$ and $\epsilon$ defined by equations (43) and (44), respectively, allows for determining whether a given system configuration belongs to the region of stable solutions or whether parametric resonance occurs. The most significant influence on the value of the parameter $\delta$ is the frequency of the exciting force $\nu$ and the value of the first natural frequency $\omega$. The system is least stable when the value of the parameter $\delta$ is approximately equal to 0.25, as shown in Fig. 3. The value of the parameter $\delta$ is also influenced by external damping $C_E$ and internal damping ${E_i}^*$. The same damping influences the reduction of unstable areas, shown in Fig. 3, by increasing the value of the coefficient $c$ described by equation (42). The value of the coefficient $\epsilon$ described by equation (44) is mainly determined by the excitation frequency $\nu$ and the value of the variable part of the load $S$. Structural damping does not affect the narrowing of the unstable-solution regions on the Strutt card.

First, a dynamic stability analysis was performed for an undamped truck crane boom system with a load of $m = 3000$ kg, a load pick-up speed of $v_0 = 0.14$ m/s, and a rigging length from the boom head to the block of $l_l = 4$ m. The values of the Mathieu equation parameters determining the dynamic stability of the solution for the analyzed geometric configurations of the system were determined (Table 1). For the assumed load and rope length in one case ($l_c = 15$ m and $\varphi = 60$), the occurrence of parametric resonance was observed. Next, the range of unstable solutions for this configuration was examined for angles

**Table 1**
Dynamic stability of selected geometric configurations of the undamped truck crane boom change system

| $l_c$ | $\varphi$ | $\delta$ | $\epsilon$ | $\nu$ | $\omega$ | Solution |
|---|---|---|---|---|---|---|
| 12 | 40° | 0.661 | 0.069 | 263.815 | 214.357 | stable |
| 12 | 60° | 0.667 | 0.015 | 263.815 | 215.461 | stable |
| 15 | 40° | 0.169 | 0.121 | 261.314 | 107.415 | stable |
| 15 | 60° | 0.257 | 0.078 | 261.314 | 132.620 | unstable |

ranging from 50° to 70°. Figures 4 and 5 show the values of the parameters $\delta$ and $\epsilon$ depending on the boom inclination angle $\varphi$. The range of angles (from 55.72° to 60.98°) for which the solution of the Mathieu equation was unstable is marked in gray.

With the increase in the boom inclination angle, the value of the parameter $\delta$ increased (Fig. 4), while the value of the parameter $\epsilon$ decreased (Fig. 5). The range of the parameter $\delta$ values corresponded to the range of the first unstable region of the solution space of the Mathieu equation. The center of the unstable region occurred at $\varphi = 58.3°$ and was adopted for further analysis of the system. As in the case of the boom inclination angle, a study was carried out of the effect of the load mass on the values of the parameters $\delta$ (Fig. 6) and $\epsilon$ (Fig. 7) of the Mathieu equation, and consequently their effect on the stability of the system.

As the load mass increased, a linear increase in the values of the parameters $\delta$ and $\epsilon$ was observed. Parametric resonance was observed for load mass values from 2900 kg to 3400 kg. The center of the unstable region occurred for the parameter value $\delta = 0.2557$ at a load mass of $m = 3150$ kg, and this value of the load mass was assumed when analyzing the effect of rope length on the values of the corresponding parameters of the Mathieu equation (Fig. 8 and Fig. 9). As the rope length increased, the values of the $\delta$ and $\epsilon$ parameters increased. An unstable region was observed in the rope length range from 3.55 m to 4.25 m, centered at a rope length of 3.9 m.

The final stage of the research was to determine the effect of different types of damping on the dynamic stability of the truck crane boom change system. The resulting unstable system for selected values of the operating angle, load mass, and rope length was subjected to external damping (Fig. 10).

As the external damping coefficient $N_S$ increased, a slight increase in system stability was observed due to a decrease in the value of the parameter $\epsilon$ (Fig. 10). However, increasing the

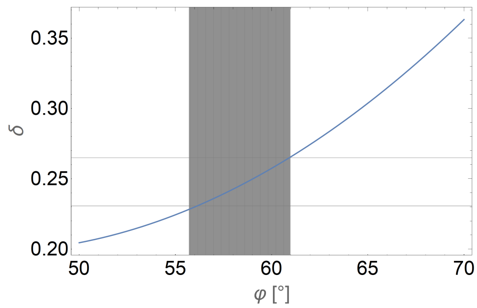


**Fig. 4.** Influence of the boom inclination angle on the value of the $\delta$ parameter with the range of angles for unstable solutions marked

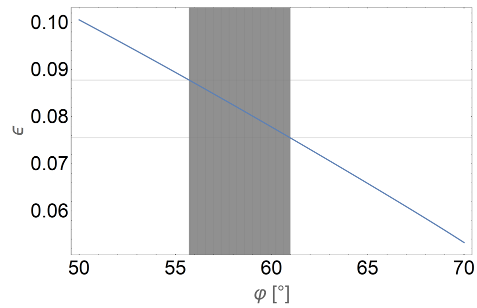


**Fig. 5.** Influence of the boom inclination angle on the value of the $\epsilon$ parameter, with the range of angles for unstable solutions marked

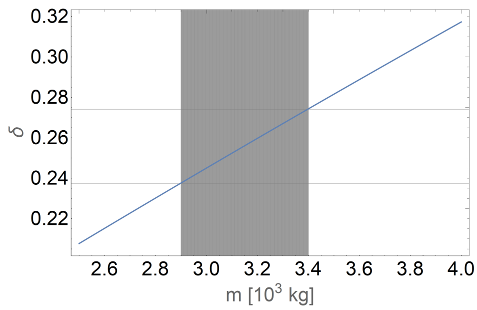


**Fig. 6.** Effect of load mass on the value of the $\delta$ parameter, with the load mass range for unstable solutions indicated

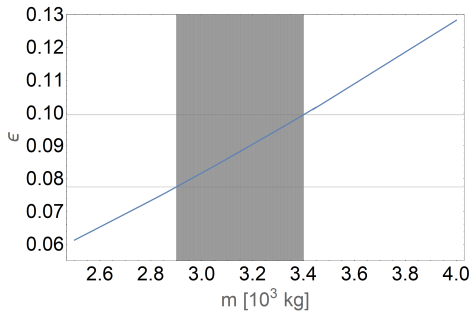


**Fig. 7.** Effect of load mass on the value of the $\epsilon$ parameter, with the load mass range for unstable solutions indicated

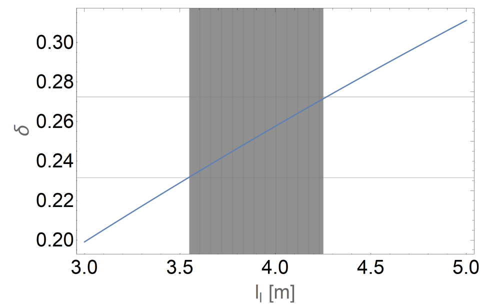


**Fig. 8.** Effect of rope length on the value of the $\delta$ parameter, with the rope length range for unstable solutions indicated

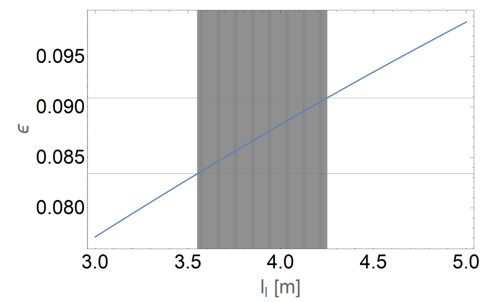


**Fig. 9.** Effect of rope length on the value of the $\epsilon$ parameter, with the rope length range for unstable solutions indicated

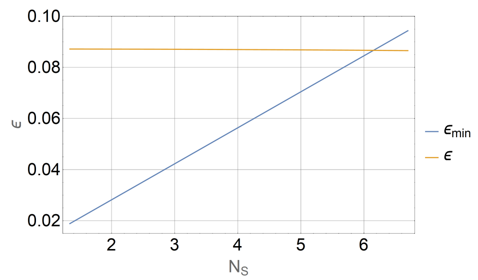


**Fig. 10.** The influence of external damping on the value of the parameter $\epsilon$ and on the value of the minimum of the unstable region $\epsilon_{\min}$

value of the damping coefficient $c$ described by equation (42) had a much greater impact on the range of unstable solutions (the unstable regions narrowed – the value $\epsilon_{\min}$ increased). For the value of the external damping coefficient $N_S = 6.15$, the curves intersected, and the system changed from unstable to stable.

Taking into account the internal damping $H_S$ (Fig. 11) slightly reduced the value of the $\epsilon$ coefficient (Fig. 11b) and increased the value of $\epsilon_{\min}$ (Fig. 11c), but this did not significantly affect the dynamic stability of the system.

The next damping type analyzed, which affected the stability of the tested system, was structural damping. The effect of this type of damping on the value of the $\epsilon$ parameter in the Mathieu equation is presented in Fig. 12.

Structural damping $M_S$, like external damping, reduced the value of parameter $\epsilon$ (Fig. 12), increasing the stability of the system to some extent. However, it did not eliminate the possibility of parametric resonance, as it did not affect the value of the damping coefficient $c$ and did not reduce the range of unstable regions ($\epsilon_{\min} = 0$).

In the final case study, the effect of all three types of damping (internal, external, and structural) on the dynamic stability of the analyzed system was considered. During the tests, internal damping was maintained at a constant value appropriate for steel ($H_S = 0.49 \cdot 10^{-4}$). The values of structural and external damping were increased proportionally until the maximum damping values adopted in the work were reached (respectively $M_S = 2.1 \cdot 10^{-2}$ and $N_S = 6.7$). The parameter that defines the proportions of the adopted dampings relative to their maximum values is the proportionality parameter $r$. The results of the tests of the influence of all types of damping on the value of the parameter $\epsilon$ from the Mathieu equation in relation to the minimum value of the unstable area $\epsilon_{\min}$ are presented in Fig. 13.

As the $r$ parameter increased, the value of parameter $\epsilon$ decreased, while the minimum value of the first unstable region $\epsilon_{\min}$ increased. Similar to Fig. 11, the curves intersected at $r = 58.87\%$, corresponding to the structural damping $M_S = 1.23 \cdot 10^{-2}$ and the external damping $N_S = 3.94$.

As can be seen, taking into account all three types of damping shifted the intersection point of the $\epsilon$ and $\epsilon_{\min}$ curves, causing the solutions to transition into stable regions earlier. A more graphical representation of the influence of internal, external, and structural damping on the range of stable solutions for the analyzed system is presented in Figs. 14a–14d.

For the obtained system, the value of the parameter $\epsilon$ for the first unstable region ($\delta = 0.25$) was tested for three different types of damping. An increase in the value of the external damping coefficient $N_S$ caused a slight increase in the system stability by reducing the value of the parameter $\epsilon$ (Fig. 10), at the same time, an increase in the value of the minimum unstable region $\epsilon_{\min}$ occurred. The system became stable for an external damping coefficient equal to $N_S = 6.15$. Internal damping $H_S$ (Fig. 11) did not significantly affect the system stability. Structural damping $M_S$ lowered the value of the parameter $\epsilon$ (Fig. 12), but did not eliminate the possibility of parametric resonance, because it did

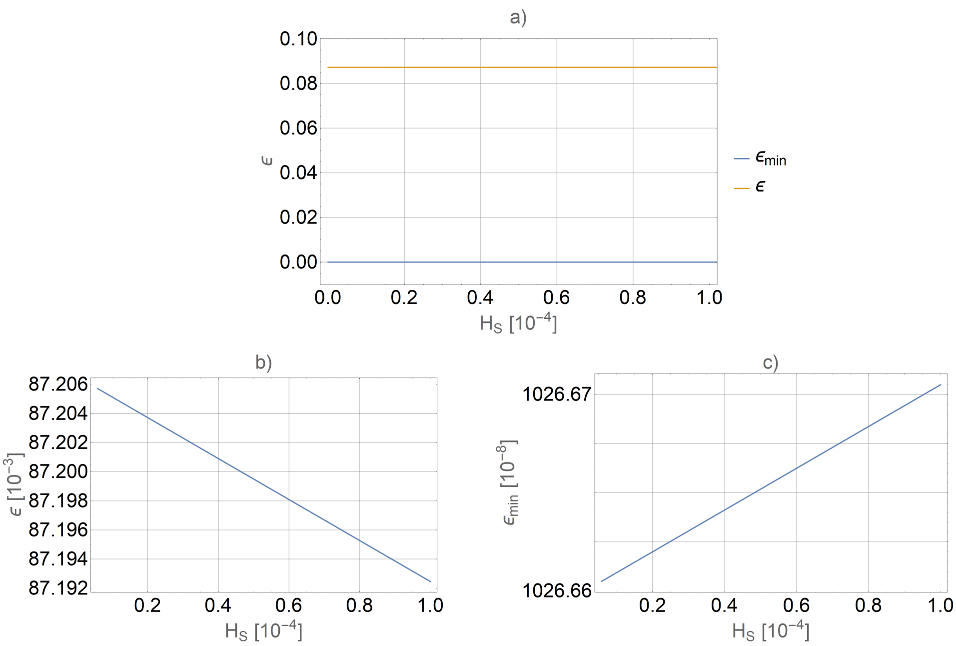


**Fig. 11.** Effect of internal damping on (a), (b) the value of the parameter $\epsilon$ and on (a), (c) the value of the minimum unstable region $\epsilon_{\min}$

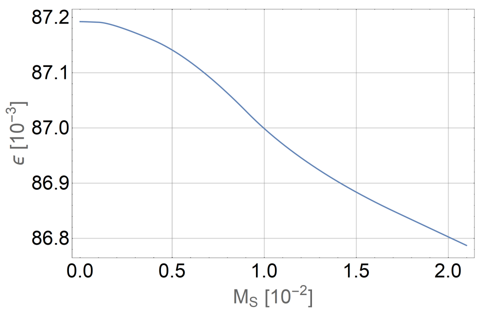


**Fig. 12.** Effect of structural damping on the value of parameter $\epsilon$

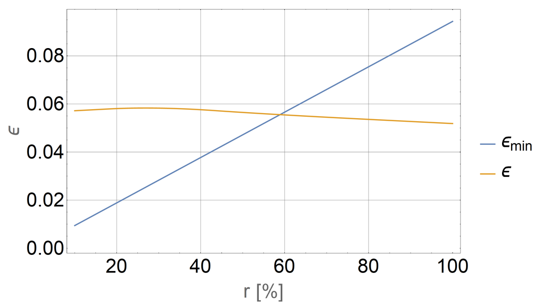


**Fig. 13.** The effect of internal, external, and structural damping on the value of parameter $\epsilon$ and on the minimum value of the unstable region $\epsilon_{min}$

not reduce the range of unstable regions. Taking into account the three types of damping made the system more stable. It became stable for the values of external damping $N_S = 3.94$ and structural damping $M_S = 1.23 \cdot 10^{-2}$, which corresponded to $r = 58.87\%$ (Fig. 13). Each additional increase in damping made the system dynamic stability solutions stable. These solutions were located entirely within the stable solution regions on the Strutt card (Fig. 14).

## 4. CONCLUSIONS

Based on the conducted research, the following conclusions were drawn:

1. Including the damping medium in the tested system reduced the areas of unstable solutions.
2. Increasing the external damping coefficient above a certain threshold ensures that the system has stable solutions throughout the analyzed range.
3. Internal damping, as modeled by the actual values of the internal damping coefficient of steel, did not introduce significant changes in dynamic stability compared to undamped systems.
4. Simultaneous consideration of all analyzed damping types significantly improved the ability to obtain stable solutions for the tested systems. These solutions, with the same geometric parameters and system loads, previously reached the stable solution region when considering single damping types.

This paper demonstrates that including damping in the truck crane boom change system does not eliminate the possibility of parametric resonance, although it significantly reduces the area of unstable solutions.


## ACKNOWLEDGEMENTS

This publication was financed by the Ministry of Education and Science of Poland as the statutory financial grant of the Department of Mechanics and Machine Design Fundamentals of Czestochowa University of Technology.


## REFERENCES


[1] B. Posiadała, D. Cekus, and R. Wilczak, *Modeling, model identification and dynamics studies of mobile cranes*. Warszawa: WNT, 2005.


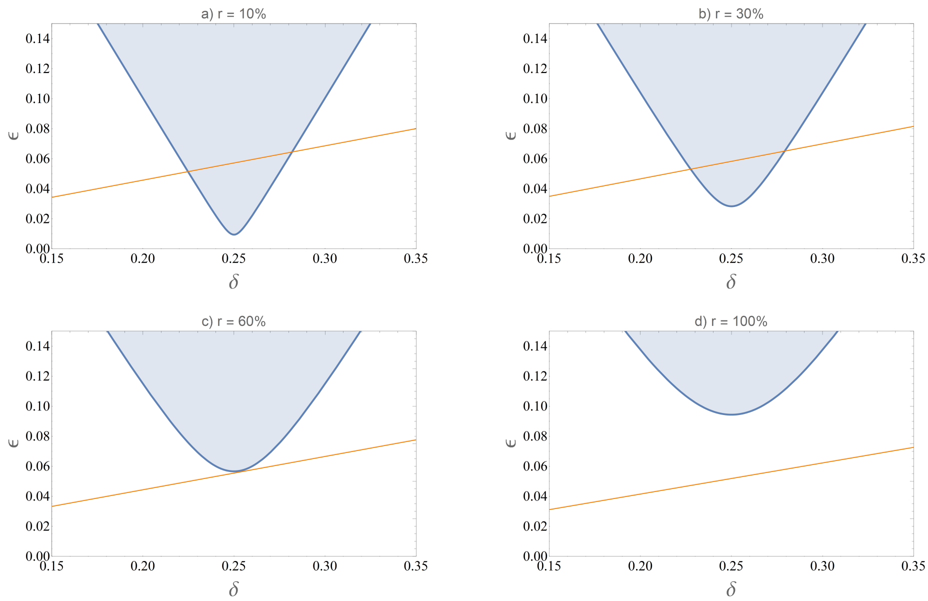


**Fig. 14.** The effect of internal, external, and structural damping on the range of stable solutions for the analyzed system

[2] W. Sochacki, *Dynamic stability of continuous-discrete damped vibrating systems: a monograph*. Częstochowa: Wydawnictwo Politechniki Częstochowskiej, 2024.

[3] D. Cekus, R. Gnatowska, and P. Kwiatoń, "Impact of wind on the movement of the load carried by rotary crane," *Appl. Sci.*, vol. 9, no. 18, p. 3842, 2019, doi: 10.3390/app9183842.

[4] A. Trąbka, "Dynamics of telescopic cranes with flexible structural components," *Int. J. Mech. Sci.*, vol. 88, pp. 162–174, 2014, doi: 10.1016/j.ijmecsci.2014.07.009.

[5] A. Sağirli, M.E. Boğoçlu, and V.E. Ömürlü, "Modeling the dynamics and kinematics of a telescopic rotary crane by the bond graph method: Part ii," *Nonlinear Dyn.*, vol. 33, no. 4, pp. 353–367, 2003, doi: 10.1023/b:nody.0000009929.80965.3b.

[6] Y. Zheng and D. Wang, "Dynamic model studies of telescopic crane with a lifting and pulling load movement," *Wirel. Pers. Commun.*, vol. 102, no. 2, pp. 753–767, 2017, doi: 10.1007/s11277-017-5098-y.

[7] S. Esqué, A. Raneda, and A. Ellman, "Techniques for studying a mobile hydraulic crane in virtual reality," *Int. J. Fluid Power*, vol. 4, no. 2, pp. 25–35, 2003, doi: 10.1080/14399776.2003.10781163.

[8] M. B. Kjelland and M. R. Hansen, "Using input shaping and pressure feedback to suppress oscillations in slewing motion of lightweight flexible hydraulic crane," *Int. J. Fluid Power*, vol. 16, no. 3, pp. 141–148, 2015, doi: 10.1080/14399776.2015.1089071.

[9] W. Sochacki, "The dynamic stability of a laboratory model of a truck crane," *Thin-Walled Struct.*, vol. 45, no. 10–11, pp. 927–930, 2007, doi: 10.1016/j.tws.2007.08.023.

[10] R. Mijailović, "Modelling the dynamic behaviour of the truck-crane," *Transport*, vol. 26, no. 4, p. 410–417, 2012, doi: 10.3846/16484142.2011.642946.

[11] R. Mijailovic and R. Selmic, "Influence of angular ball bearing deformation on truck-crane dynamic stability," *Facta Univ. Ser. Mech. Eng.*, vol. 2, no. 9, pp. 1129–1143, 2004.

[12] G. Sun and M. Kleeberger, "Dynamic responses of hydraulic mobile crane with consideration of the drive system," *Mech. Mach. Theory*, vol. 38, no. 12, p. 1489–1508, 2003, doi: 10.1016/s0094-114x(03)00099-5.

[13] D. Ilir and L. Naser, "Truck mounted cranes during load lifting – dynamic analysis and regulation using modelling and simulations," *Int. Sci. J. Mach. Technol. Mater.*, vol. 8, pp. 12–15, 2016.

[14] S. Liu, J. Liu, K. Zhang, and L. Meng, "The dynamic stability analysis of telescopic booms of the crane based on the energy method," *IOP Conf. Ser. Mater. Sci. Eng.*, vol. 399, p. 012033, 2018, doi: 10.1088/1757-899x/399/1/012033.

[15] M. Bold, S. Garus, and W. Sochacki, "Damped vibrations of telescopic crane boom," in *Engineering Mechanics 2018*, ser. EM2018. Institute of Theoretical and Applied Mechanics of the Czech Academy of Sciences, 2018, pp. 101–104, doi: 10.21495/91-8-101.

[16] I.G. Raftoyiannis and G.T. Michaltsos, "Dynamic behavior of telescopic cranes boom," *Int. J. Struct. Stab. Dyn.*, vol. 13, no. 01, p. 1350010, 2013, doi: 10.1142/s0219455413500107.

[17] A. Maczynski and S. Wojciech, "Dynamics of a mobile crane and optimisation of the slewing motion of its upper structure," *Nonlinear Dyn.*, vol. 32, no. 3, pp. 259–290, 2003, doi: 10.1023/a:1024480318414.

[18] W. Kacalak, Z. Budniak, and M. Majewski, "Stability assessment as a criterion of stabilization of the movement trajectory of mobile crane working elements," *Int. J. Appl. Mech. Eng.*, vol. 23, no. 1, pp. 65–77, 2018, doi: 10.1515/ijame-2018-0004.

[19] H.D. Tran and N.S. Nguyen, "Identification of the dynamic stability of truck cranes," *EUREKA Phys. Eng.*, no. 3, pp. 130–142, 2025, doi: 10.21303/2461-4262.2025.003641.

[20] A. Mackojć and B. Chiliński, "Preliminary modelling methodology of a coupled payload-vessel system for offshore lifts of light and heavyweight objects," *Bull. Pol. Acad. Sci. Tech. Sci.*, p. 139003, 2022, doi: 10.24425/bpasts.2021.139003.

[21] J.B. Qian, L.P. Bao, R.B. Yuan, and X.J. Yang, "Modeling and analysis of outrigger reaction forces of hydraulic mobile crane," *Int. J. Eng.*, vol. 30, pp. 1246–1252, 2017, doi: 10.5829/ije.2017.30.08b.18.

[22] L.-K. Chou and M.-X. Lin, "Analysis of Bernoulli–Euler beam on nonlinear elastic foundation using the Modified Adomian Decomposition Method," *Eng. Comput.*, vol. 43, no. 2, pp. 746–769, 2026, doi: 10.1108/EC-06-2025-0587.

[23] E.Z. Sensoy and T. Baran, "Modal Analyses of Non-Uniform Axially Functionally Graded Euler-Bernoulli Beams," *Bull. Pol. Acad. Sci. Tech. Sci.*, p. 157320, 2025, doi: 10.24425/bpasts.2026.157320.

[24] S. Zhao, L. Li, and P. Shi, "Analytical solutions of functionally graded microbeam models based on the modified couple stress theory: A comparative study of Euler-Bernoulli, Timoshenko and Reddy beams," *Thin-Walled Struct.*, vol. 224, p. 114648, 2026, doi: 10.1016/j.tws.2026.114648.

[25] N. Challamel and A. Aftabi-Sani, "Vibration and stability of two-phase peridynamic Euler-Bernoulli beams under general boundary conditions – Exact and numerical approaches," *Eur. J. Mech. A Solids*, vol. 117, p. 105993, 2026, doi: 10.1016/j.euromechsol.2025.105993.

[26] K. Misiurek, M. Podwórna, P. Ruta, O. Szyłko-Bigus, and R. Idzikowski, "Static analysis of a two-layer beam with a flexible interlayer connection," *Bull. Pol. Acad. Sci. Tech. Sci.*, p. 154278, 2025, doi: 10.24425/bpasts.2025.154278.

[27] T. Geisler and W. Sochacki, "Modelling and research into the vibrations of truck crane," *Sci. Res. Inst. Math. Comput. Sci.*, vol. 10, no. 1, pp. 49–60, 2011.

[28] B. Posiadała (ed.), *Research and identification of dynamic models of a laboratory crane*. Warszawa: FKNT, WNT, 2005.

[29] P. Francis, "Parametric excitation of a non-homogeneous Bernoulli-Euler beam," *J. Mech. Eng. Sci.*, vol. 10, no. 3, pp. 205–212, 1968, doi: 10.1243/jmes_jour_1968_010_032_02.

[30] T. Yan, S. Kitipornchai, and J. Yang, "Parametric instability of functionally graded beams with an open edge crack under axial pulsating excitation," *Compos. Struct.*, vol. 93, no. 7, pp. 1801–1808, 2011, doi: 10.1016/j.compstruct.2011.01.019.